Tribol Lett (2012) 48:95–102
DOI 10.1007/s11249-012-0002-0

ORIGINAL PAPER

Triggering Frictional Slip by Mechanical Vibrations

Rosario Capozza · Andrea Vanossi · Alessandro Vezzani · Stefano Zapperi

Received: 15 December 2011 / Accepted: 19 June 2012 / Published online: 7 July 2012

Abstract We study the slippage of a tribological system of particles confined between a horizontally driven top plate and a vertically oscillating bottom plate. As shown in a recent article (Capozza et al., Phys Rev Lett 103:085502, 2009), tiny vibrations, when applied in a suitable range of frequencies, may suppress the high dissipative stick–slip dynamics reducing drastically the lateral friction force. Here, we generalize and prove the robustness of the results against the effect of quenched disorder in the confining substrates and the presence of adhesive and cohesive forces at the interface. The observed phenomenology is shown to hold true by moving from the previously considered two dimensional modeling to a more realistic three dimensional geometry. A detailed analysis is devoted to the case of short vibration pulses. These findings are relevant for nanoscale mechanics and in the context of earthquake or avalanches triggering.

Keywords Mechanical control of friction · Friction mechanisms · Stick–slip · Numerical simulations

R. Capozza (✉)
School of Chemistry, Tel Aviv University, 69978 Tel Aviv, Israel
e-mail: rosario.capozza@gmail.com

A. Vanossi
Consiglio Nazionale delle Ricerche CNR-IOM Democritos and International School for Advanced Studies (SISSA), Via Bonomea 265, I-34136 Trieste, Italy
e-mail: vanossi@sissa.it

A. Vezzani
Dipartimento di Fisica, Università degli Studi di Parma, Viale G.P. Usberti 7/A, 43100 Parma, Italy
e-mail: vezzani@fis.unipr.it

A. Vezzani
Consiglio Nazionale delle Ricerche CNR-NANO S3, Via Campi 213A, 41125 Modena, Italy

S. Zapperi
Consiglio Nazionale delle Ricerche CNR-IENI, Via R. Cozzi 53, 20125 Milan, Italy
e-mail: stefano.zapperi@cnr.it

S. Zapperi
ISI Foundation, Viale S. Severo 65, 10133 Turin, Italy

1 Introduction

Understanding the mechanisms that can reduce friction and facilitate the slippage of two surfaces in contact is of fundamental interest and practical importance for nanoscale systems as well as for macroscale ones [1, 2]. The energy accumulated during the stick phase, when the surfaces are interlocked together, is released at the interface during the slip event as soon as the driving force overcomes the static friction threshold. This sticking/slipping alternation is responsible for serious limitations on the performance and lifetime of technological micro devices (due, e.g., to wear and debris) but also dictates, on much larger macroscopic scales, the occurrence of catastrophic events, like earthquakes between geological faults. The strain energy release at the interface may follow different dissipative paths, ranging from single sudden catastrophic jumps to much slower tiny multiple slips. Many factors may indeed influence the slip phase. The temperature can, for example, decrease the slip length of a nanometric tip resulting in a rich temperature dependence of friction [3–6]. It has also been observed in different tribological systems, both numerically [6–10] and experimentally [11–14], that small mechanical vibrations, when applied at suitable frequency and amplitude ranges may increase surface mobility and diffusion or, as in sheared granular

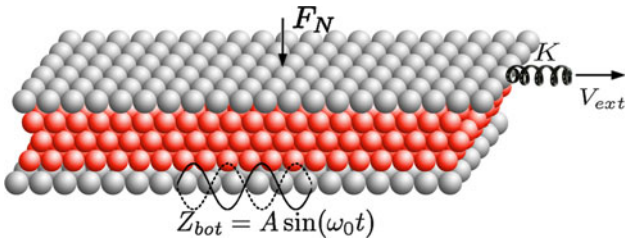

Fig. 1 (Color online) Sketch of the confined system geometry used in MD simulations. The *top plate*, subject to a normal load F_N, is driven through a spring $K = 1.5 \times 10^{-2}$, moving at constant velocity $V_{ext} = 0.01$; the *bottom plate* vibrates vertically with frequency ω_0 and small amplitude A

media experiments, perturb the intermittent dynamics by *triggering* small amplitude stick–slip events [15]. Despite these promising numerical and experimental contributions, a detailed analysis accounting for the friction dependence on vibrations is still partially lacking.

In this article, we briefly review and significantly generalize and extend the recent theoretical and computational results concerning the suppression of friction by tiny mechanical oscillations in a bounded system under shear [16]. As sketched in Fig. 1, the top plate, confining a certain number of particle layers, is attached to a spring moving at constant speed, while the bottom plate is vibrated vertically. At low pulling velocities without any applied oscillation, the top plate exhibits a characteristic stick–slip regime [17, 18]. In a well-defined frequency range, small normal vibrations are shown to induce a drastic reduction of the friction coefficient, with the consequent disappearance of the high dissipative intermittent dynamics. We find that these results can be generalized in the presence of quenched disorder in the confining substrates and for different type of forces (repulsive, adhesive, and cohesive) characterizing the particle interactions of the model. The observed phenomenology is shown to hold true by moving from the previously considered two dimensional (2D) modeling to a more complex three dimensional (3D) system. Besides, under a small external stress (smaller than the static threshold), the vibration-induced suppression of friction turns out to be accompanied by a slippage whose length, unexpectedly, is not increasing monotonically with the applied lateral force.

The paper is organized as follows. In Sect. 2, we introduce the model used for our simulations, elucidating some computational details; we review the tribological phenomenology and the theoretical explanation of the numerical results for the observed suppression of friction, as previously reported in [16]. In Sect. 3, we prove the robustness of our results against the effect of quenched disorder in the confining substrates and the presence of adhesive and cohesive forces at the interface. Sect. 4 shows that an increase of the system diffusivity takes place at the interface in the same range of oscillation frequencies where the frictional drop manifests itself. In Sect. 5, we extend the molecular dynamics (MD) simulations to a more realistic 3D geometry. Sect. 6 analyzes the case of vibration pulses acting for a small amount of time as in the case of earthquakes or avalanches triggered by seismic waves. Conclusions are given in Sect. 7.

2 Model, Phenomenology, and Friction Suppression

Let us first introduce the 2D tribological model [16] consisting of two identical (and rigid) top and bottom substrates, composed of $n_t = n_b$ particles with coordinates $\boldsymbol{r}_i^t$ and $\boldsymbol{r}_i^b$ respectively and constant lattice separation a_s=1. We confine n_p particles with coordinates $\boldsymbol{r}_i^p$ between the top and bottom plates. Periodic boundary conditions are applied along the x-shearing direction. All the particles in the system have the same mass m and interact via the same Lennard–Jones (LJ) pairwise potential $U(r) = U_0\left[\left(\frac{r_0}{r}\right)^{12} - 2\left(\frac{r_0}{r}\right)^{6}\right]$ for $r < r_c$ and $U(r) = 0$ otherwise. To simulate repulsive interactions, we set $r_c = r_0$, effectively canceling the LJ attractive contribution. Particle cohesion and adhesion with the substrates are switched on by setting the corresponding $r_c \to \infty$.

By imposing $n_p = N_l \cdot n_t = N_l \cdot n_b$ with N_l an integer number, the system forms N_l perfectly ordered confined layers. However, we have also considered cases of a few missing particles, finding similar results as long as the system remains ordered. The top plate, subject to a normal force F_N, is pulled along x at constant velocity V_{ext} through a spring K (Fig. 1). Indicating with $\boldsymbol{R}_{top} = (X_{top}, Z_{top})$ and $\boldsymbol{R}_{bot} = (X_{bot}, Z_{bot})$ the center of mass coordinates of the top and bottom plate, respectively, the confined particles satisfy the equations of motion

$$m\ddot{\boldsymbol{r}}_i^p + \sum_{i\neq j}^{N} \frac{\mathrm{d}}{\mathrm{d}\boldsymbol{r}_i} U(|\boldsymbol{r}_i^p - \boldsymbol{r}_j|) + m\eta(\dot{\boldsymbol{r}}_i^p - \dot{\boldsymbol{R}}_{top}) + m\eta(\dot{\boldsymbol{r}}_i^p - \dot{\boldsymbol{R}}_{bot}) + \boldsymbol{f}^{ran} = 0, \tag{1}$$

while the top plate dynamics is described by

$$M_{top}\ddot{X}_{top} + \sum_{i=1}^{n_t}\sum_{j=1}^{n_p} \frac{\mathrm{d}}{\mathrm{d}x_i^t} U(|\boldsymbol{r}_j^p - \boldsymbol{r}_i^t|) + K(X_{top} - V_{ext}t) + \sum_{i=1}^{n_p} m\eta(\dot{X}_{top} - \dot{x}_i^p) + f_x^{ran} = 0, \tag{2}$$

$$M_{top}\ddot{Z}_{top} + \sum_{i=1}^{n_t}\sum_{j=1}^{n_p} \frac{\mathrm{d}}{\mathrm{d}z_i^t} U(|\boldsymbol{r}_j^p - \boldsymbol{r}_i^t|) + F_N + \sum_{i=1}^{n_p} m\eta(\dot{Z}_{top} - \dot{z}_i^p) + f_z^{ran} = 0, \tag{3}$$

where $N = n_p + n_t + n_b$, and η is the damping coefficient that accounts for a viscous dissipation [19, 20].

The temperature is controlled by a Langevin thermostat according to the fluctuation/dissipation relation $\langle \boldsymbol{f}_i(t)^{\mathrm{ran}} \boldsymbol{f}_j(t')^{\mathrm{ran}} \rangle = 4m\eta k_{\mathrm{B}} T \delta_{ij} \delta(t-t')$. Having in mind here a very simplified description of a mesoscopic system (such as, e.g., a granular medium), we just consider very low temperature values ($k_{\mathrm{B}}T = 10^{-2}\ U_0$).

To study the influence of mechanical oscillations, the bottom plate coordinate Z_{bot} is vibrated vertically with amplitude A and frequency ω_0, while the horizontal component X_{bot} is held fixed. We compute the instantaneous friction coefficient by measuring the spring elongation $\mu = K\,(X_{\mathrm{top}}(t) - V_{\mathrm{ext}}t)/F_{\mathrm{N}}$, and its average $\langle \mu \rangle$, obtained by integrating its value over a sufficiently long time interval in the steady state.

Without any oscillations, a typical stick–slip behavior appears, with loading phases where the system is at rest, followed by rapid slip events in which the force accumulated by the spring is relaxed. A systematic calculation of the average friction coefficient $\langle \mu \rangle$ versus the vibration frequency ω_0 is reported in Fig. 2a. This panel shows results obtained for various oscillation amplitudes A, ranging from 3 to 9 % of the film thickness. Very similar trends are obtained by varying ω_0 in correspondence of different values of the damping coefficient η and different numbers of confined layers. At low frequencies, the top plate and the confined particles vibrate in phase with the oscillations of the bottom plate. At $\omega_0 = 2$, instead, the top plate and the confined particles cannot follow the bottom substrate dynamics. Here, the vertical position of the top plate increases, presenting high amplitude oscillations which diminish the contact time between the confined particles and the bottom plate, reducing considerably the friction resistance. In the context of reference [8], this situation corresponds to an increase of the system dilatacy leading to a decrease of frictional force. Further increases of the frequency ω_0 induce a reduction of the amplitude of the top plate oscillations around the equilibrium position; as a result, the friction force rises again to higher values.

This phenomenology shares similarities with the physics of the bouncing-ball problem [21–23] and in particular with its 2D version referred to as the bouncing-ball billiard [24, 25]. In fact, in analogy with the bouncing-ball problem, there is a range of low frequencies for which the ball does not bounce but remains stuck to the bottom plate. For higher frequencies, it starts to hop with the period of the driving. With a further increase of ω_0 there is period doubling, and eventually a transition to chaos that has been related, in the bouncing-ball billiard to diffusion. We also observe in our system a diffusive behavior (Sect. 4).

The results suggest an argument to derive analytically the values ω_1 and ω_2, defining the frequency window of suppression of friction. The frictional behavior is determined by the competition between the inertial forces induced in by the oscillations and the load.

The reduction of friction occurs when the particles are able to detach from the bottom plate due to the action of the vertical inertial force $F_{\mathrm{in}} = M\ddot{Z}_{\mathrm{bot}} \simeq MA\omega_0^2$ induced by the

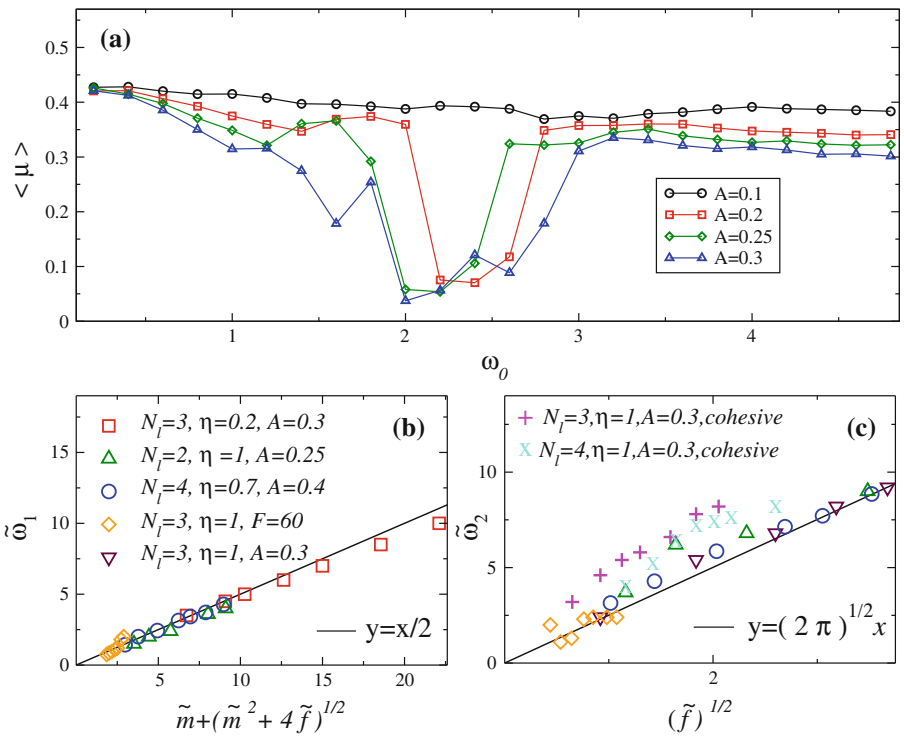

Fig. 2 **a** Time-averaged value of μ as a function of ω_0 for four values of the oscillation amplitude A (ranging from 3 to 9 % of the $N_{\mathrm{l}} = 3$ lubricant thickness). Comparison between the numerical results (*symbols*) and the theory (*solid line*): **b** $\tilde{\omega}_1$ as a function of the dimensionless variables $\tilde{f}$ and $\tilde{m}$; **c** $\tilde{\omega}_2$ as a function of $\tilde{f}$. The behaviors corresponding to *different symbols* are obtained keeping three parameters fixed and varying the fourth. The *symbols* (+) and (x) refer to the cohesive case

external vibrations, where $M = M_p + M_{top}$. The frequency ω_1 corresponds to the condition for which this inertial force overcomes the combined action of the normal load F_N and the damping force $F_{damp} = M_p \eta \dot{Z}_{bot} \simeq M_p \eta A \omega_0$, i.e.,

$$F_{in}(\omega_1) \simeq F_N + F_{damp}(\omega_1). \quad (4)$$

Introducing the rescaled dimensionless variables

$$\tilde{f} \equiv \frac{F_N}{MA\eta^2}, \quad \tilde{m} \equiv \frac{M_p}{M}, \quad \tilde{\omega} \equiv \frac{\omega}{\eta}, \quad (5)$$

we obtain for the starting frequency of friction suppression

$$\tilde{\omega}_1 = \frac{1}{2}\left(\tilde{m} + \sqrt{\tilde{m}^2 + 4\tilde{f}}\right). \quad (6)$$

The recovery frequency ω_2 is determined by an external mechanical actuation fast enough to reduce the amplitude of the top plate oscillations, because of the presence of low frequency vibrations suppressing the relevant resonant peaks [16]. Comparing the vibration-induced characteristic detachment time of the confined layers from the bottom plate,

$$\Delta t \simeq \dot{Z}_{bot} M / F_N \simeq A\omega_0 M / F_N, \quad (7)$$

to the external oscillation period $2\pi/\omega_0$, we end up (using 5), with

$$\tilde{\omega}_2 = \sqrt{2\pi\tilde{f}}. \quad (8)$$

The theoretical predictions for ω_1 and ω_2 are in excellent agreement with the numerical simulations as shown in Fig. 2b, c. The numerical values are obtained varying the number of layers N_l, the vibration amplitude A, the damping coefficient η and the normal load F_N. Based on the relations (6) and (8), a phase diagram indicating the region of suppressed friction in the space $(\tilde{f}, \tilde{\omega})$ can be easily obtained [16].

A frequency range where friction suppression is observed can be estimated considering the experiment [26], where a granular medium was confined between two plates sheared at constant velocity. We obtain $\omega_1 \simeq$ 44 Hz and $\omega_2 \simeq$ 111 Hz for the parameter values $M_{top} =$ 0.75, $M_p = 0.5$ kg, $\eta = 0.0076$ s^{-1} and an amplitude of vibration $A = 0.005$ m.

3 Surface Interactions and Disorder

We have verified the validity of our results for different surface interactions and spatial configurations: attractive forces among the confined particles (cohesion), among particles and substrates (adhesion), and substrate quenched disorder. The effect of the various kinds of interaction on the friction coefficient μ is reported in Fig. 3, showing the behavior of $\langle\mu\rangle$ versus ω_0 renormalized to the corresponding average friction coefficient μ_0 in the absence of vibrations. In all these cases, we find again that friction is suppressed in a well-defined frequency range.

The presence of particle cohesion does increase only the frequency ω_2 as shown in Fig. 3 (circle black curve) and in Fig. 2c, where the values of $\tilde{\omega}_2$ for the cohesive case ("+" and "x" symbols) are shifted up respect to the theoretical solid line. A larger value of ω_2 can be here explained qualitatively in terms of the larger efficiency in transferring the impulse I to the sliding system by the bottom substrate oscillations. In fact, above ω_1 and in the absence of attractive forces

$$I = \begin{cases} \int_t^{t+\Delta t_p} F_{in} dt & \text{if } \ddot{Z}_{bot} > 0; \\ 0 & \text{if } \ddot{Z}_{bot} \leq 0 \end{cases}$$

where $F_{in} = M_{eff}\ddot{Z}_{bot}$ represents the inertial force acting on the top plate and confined particles and M_{eff} is the mass of the system interacting effectively with the bottom surface during the interval of time Δt_p characterized by the positive substrate acceleration $\ddot{Z}_{bot} > 0$. In general $M_{eff} < M (= M_p + M_{top})$, however, thanks to the cohesive interaction, the system exhibits a more compact structure during the upward thrust and M_{eff} turns to be of the order of the whole mass $M_p + M_{top}$. In the repulsive case, on the contrary, the confined particles tend to dilate after each interactive lift with the bottom plate and become again compact in a typical time τ_r. In such a situation, if $\Delta t_p < \tau_r$, the confined particles do not have enough time to re-aggregate and only a fraction of them will readily respond to the next upward substrate boost, implying $M_{eff} < M_{top} + M_p$, and hence $I^{rep} < I^{cohes}$, i.e., the impulse transferred is here smaller than in the cohesive case.

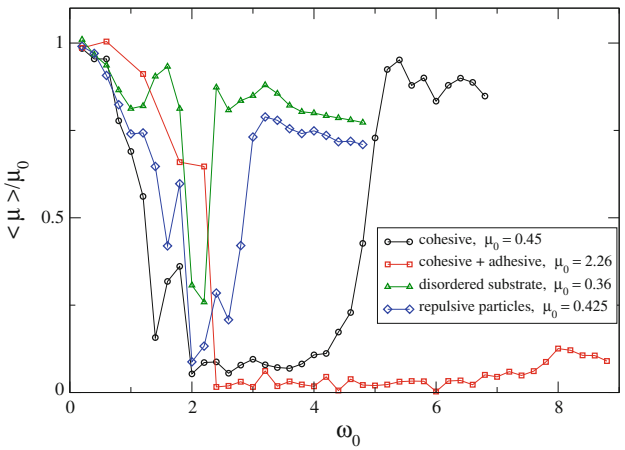

Fig. 3 Simulations with attractive interparticle forces (cohesive), adhesive forces with the substrates (cohesive + adhesive), and disordered substrates. The *blue curve* shows the case of repulsive particles. μ_0 is the average friction coefficient for $\omega_0 = 0$. $\langle\mu\rangle / \mu_0$ as a function of ω_0. Here, $M_{top} = 60$, $M_p = 177$, $F_N = 60$, $A = 0.3$

The dilation of confined particles ΔZ, can be characterized quantitatively by the mean square displacement of their vertical coordinate z_i respect to the center of mass coordinate $Z_{\rm cm}$, i.e., $\Delta Z = 1/n_p \sum_{i=1}^{n_p} (Z_{\rm cm} - z_i)^2$. ΔZ represents the spreading of z_i coordinates around $Z_{\rm cm}$. Figure 4 shows the behavior of ΔZ as a function of time for the repulsive and cohesive case at $\omega_0 = 2$, in the interval of friction suppression. The negative peaks of ΔZ below the equilibrium value (shown by the dash dotted horizontal line) indicates compression of particles due to the interactive lift. In the repulsive case, the downward peak is followed by a sudden increase, signaling a significant dilation of the confined layer, that recovers a compact structure after a time τ_r. In the cohesive case, the interaction with the bottom is followed by oscillations of ΔZ, indicating that particles do not spread and keep their compact structure, being ready, straightaway, to receive another effective kick from the subsequent bottom plate oscillation. On the other hand, an attractive LJ interaction between cohesive particles and substrates (adhesion) leads to a net increase of the friction coefficient in the absence of external actuation (μ_0 being about five times larger in comparison to that evaluated in the presence of the other kinds of interaction). By switching the vibrations on, we find here (see Fig. 3, square red curve) that friction is suppressed at a frequency ω_1 higher than the one corresponding to the case of purely repulsive forces. This effect is explained reasonably by our theory by adding the "loading" contribution of the adhesive force between substrates and particles. By doing so, the relation 4 becomes:

$$F_{\rm in}(\omega_1) \simeq F_{\rm N}(\omega_1) + F_{\rm damp}(\omega_1) + F_{\rm ad}. \quad (9)$$

The value of $F_{\rm ad}$ can be calculated by considering the force needed to detach vertically a single particle from a layer of immobile LJ particles. Our estimation provides us with $F_{\rm ad} = 288$, that can be considered as a further contribution to the normal load. With this value of $F_{\rm ad}$, we obtain an estimation of $\omega_1 \simeq 2.6$ that is consistent with the results obtained in our simulations. We speculate that the recovery of friction occurring at large values of ω_2 is here determined by the particular compact (adhesive) structure of the confined film and the top plate, making the mechanism of the system upward thrust (due to substrate oscillation) more effective.

We have checked the robustness of our results also in the presence of disordered confining substrates, by randomly displacing the particle positions in the substrates (up to 10 % of lattice equilibrium spacing), along the horizontal and vertical directions. In this case, we have obtained results consistent with those of crystalline substrate case. The frequency interval of friction suppression

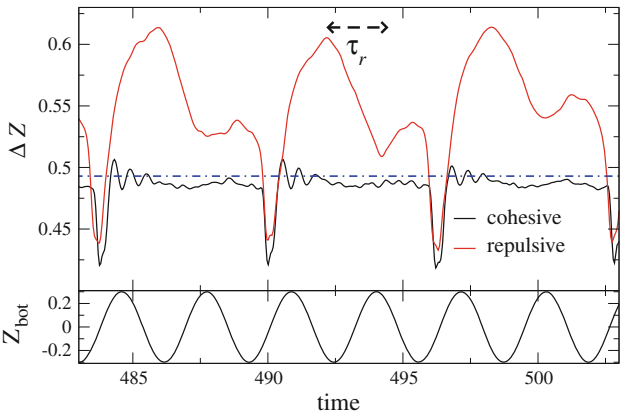

Fig. 4 Dilation ΔZ of the confined particles as a function of time in the cohesive (*black*) and repulsive (*red*) case at $\omega_0 = 2$. The *horizontal dashed dotted line* indicates the equilibrium value of ΔZ for the repulsive case

shrinks in the presence of disorder, but it remains centered in the interval ω_1 and ω_2 calculated in the absence of disorder (see Fig. 3, triangle green curve). A further increase of disorder leads to a gradual shrinking of the window up to a complete disappearance. Above a certain disorder threshold in the substrate lattice spacing, the compact crystalline structure of the confined film is basically ruined and the oscillation effectiveness lost. In addition, as previously mentioned, the results hold true in the presence of defects (i.e., vacancies) in the confined film, as long as its structure remains sufficiently ordered.

4 Diffusion Induced by Vibrations

Manipulations by mechanical excitations, when applied at suitable frequency and amplitude ranges, may help in driving an interface contacting system out of its potential energy minima, thus increasing considerably surface mobility and reducing friction. We have verified by simulations that the diffusivity of the top plate exhibits a strong enhancement in the frequency range where the suppression of lateral friction takes place. The diffusivity has been evaluated without any applied external driving and in the presence of just the bottom substrate oscillations. The mean square displacement Δr^2 of the top plate at ω_0 has been calculated by averaging the displacement of $X_{\rm top}$ at each time on many different realizations. These simulations correspond to the case of three confined layers of repulsive particles and an amplitude of oscillations $A = 0.3$. The diffusion coefficient D as a function of ω_0 is reported in Fig. 5. In the range of friction suppression D is three orders of magnitude larger (compare Fig. 5 with the diamond blue curve in Fig. 3).

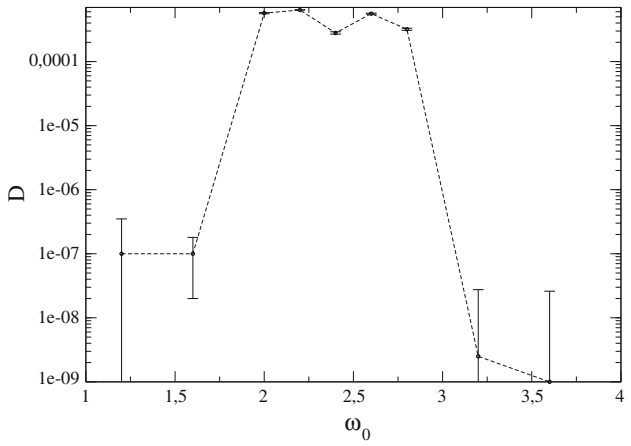

Fig. 5 Dependence of the diffusion coefficient on the vibration frequency ω_0. Here, $M_{\text{top}} = 60$, $M_{\text{p}} = 177$, $F_{\text{load}} = 60$, $A = 0.3$

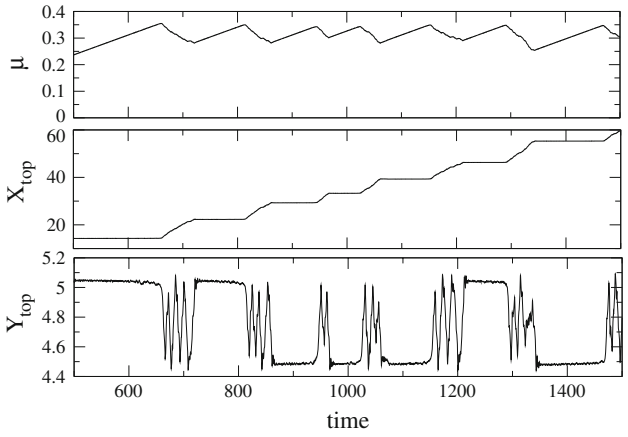

Fig. 6 3D simulations (no oscillations applied). Friction coefficient μ, X_{top} and Y_{top} as a function of time. The *top plate* proceeds with a zig–zag motion in the y direction. Here, $M_{\text{top}} = 144$, $M_{\text{p}} = 432$, $F_{\text{N}} = 288$

5 3D Simulations

The generality of our findings suggests that the results are not an artifact of the assumed 2D simple geometry and could hold true for other, more realistic, situations. Thus, we have performed additional numerical simulations for a 3D confined configuration.

To the equations of motion (1–3), that read formally the same also for the 3D case geometry, we should add the one for the y-component of the top plate:

$$M_{\text{top}}\ddot{Y}_{\text{top}} + \sum_{i=1}^{n_{\text{t}}}\sum_{j=1}^{n_{\text{p}}} \frac{\mathrm{d}}{\mathrm{d}y_i^{\text{t}}} U(|\boldsymbol{r}_j^{\text{p}} - \boldsymbol{r}_i^{\text{t}}|) + \sum_{i=1}^{n_{\text{p}}} m\eta(\dot{Y}_{\text{top}} - \dot{y}_i^{\text{p}}) + f_y^{\text{ran}} = 0. \quad (10)$$

The top plate, of mass $M_{\text{top}} = m \cdot n_{\text{t}}$ and subject to a normal load F_{N}, is pulled through a spring K moving only along x at velocity V_{ext}. Periodic boundary conditions are applied along the x and y directions.

Specifically, we have studied the case of three layers ($n_{\text{p}} = 432$) of repulsive particles confined in between two rigid planar substrates composed of $n_{\text{t}} = n_{\text{b}} = 144$ particles arranged in a triangular lattice. Here again, when the spring is dragged at a sufficiently low constant velocity V_{ext}, the top plate exhibits a typical stick–slip dynamics. The potential generated by the rigid substrates is characterized by maxima, minima and saddle points. Contrary to the 2D case, where no option exists, the top plate proceeds here, during the slip phase, moving around the maxima and passing through the smaller barrier of the saddle points. This results in a "zig–zag" motion of Y_{top} around the y coordinate (Fig. 6). This behavior is certainly influenced by the rigidity of the confined film layers. The dependence of the friction coefficient on the vibration frequency is reported in Fig. 7. The frequency values of suppression and recovery of friction ω_1 and ω_2 can be calculated

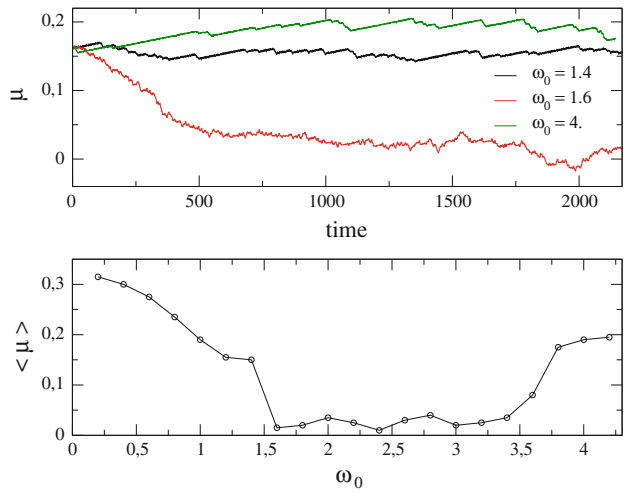

Fig. 7 3D simulations. (*Top*) μ as a function of ω_0. (*Bottom*) μ as a function of time for three values of ω_0. Here, $M_{\text{top}} = 144$, $M_{\text{p}} = 432$, $F_{\text{N}} = 288$, $A = 0.4$

considering the new values of the M, η, A and F_{N}. The theoretical estimations are again in agreement with the computational results.

6 Slippage Triggered by Impulsive Vibrations

In many cases, the external vibration acts only for a short time interval, such as at the macroscopic scales, in the case of earthquakes or avalanches triggered by seismic waves. To address this issue, we analyze the slip jump Δ_{slip} for a small vertical vibration of finite duration T_{v} and frequency ω_0, with $T_{\text{v}} \gg 1/\omega_0$. In order to limit extended time-consuming numerical simulations, and having previously

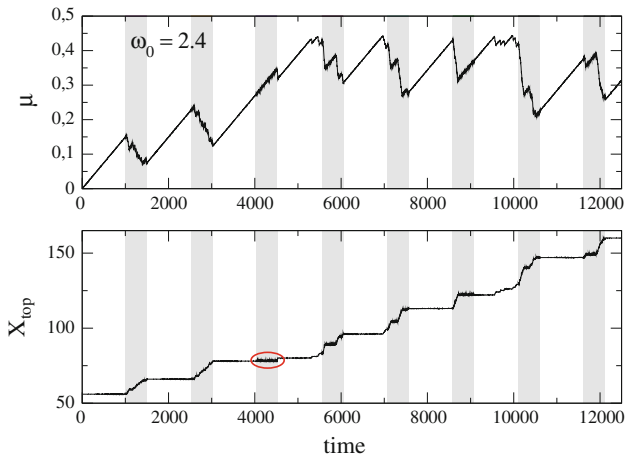

Fig. 8 Effect of multiple pulses (*grey stripes*) on μ and X_{top}. The *red circle* indicates a pulse with a minor effect on the system dynamics. Here, $M_{\text{top}} = 60$, $M_{\text{p}} = 177$, $F_{\text{load}} = 60$, $A = 0.2$

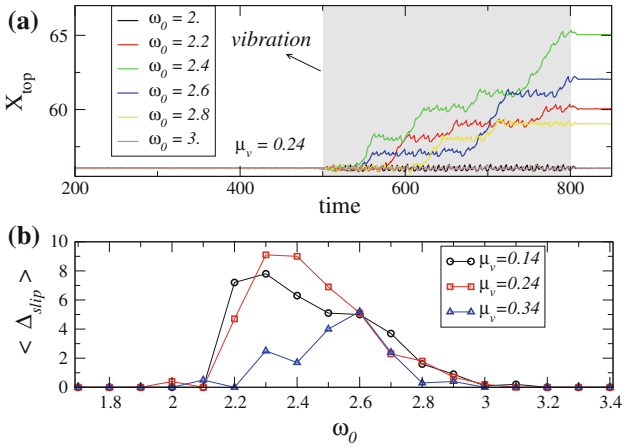

Fig. 9 **a** *Horizontal top plate* displacement as a function of time for indicated values of ω_0 in the case of $\mu_{\text{v}} = 0.24$. **b** Average slip length as a function of ω_0 for different values of μ_{v}. Here, $M_{\text{top}} = 60$, $M_{\text{p}} = 177$, $F_{\text{N}} = 60$, $A = 0.2$, $T_{\text{v}} = 300$

verified the occurrence of an almost identical tribological phenomenology related to the vibration-induced friction suppression in 3D, the analysis has been carried out here in the framework of the simpler 2D geometry. To avoid discontinuities, we switch on smoothly the perturbation on the bottom plate: $Z_{\text{bot}} = Z_0 + f(t, T_{\text{v}})A\sin(\omega_0 t)$, where $f(t, T_{\text{v}}) = (\tanh(t/\tau) - \tanh((t - T_{\text{v}})/\tau))/2$, with $\tau \ll T_{\text{v}}$. The system is first thermalized before being dragged by the spring at constant velocity. The effect of periodic pulses of frequency $\omega_0 = 2.4$ (in the interval of friction suppression) and duration $T_{\text{v}} = 500$ (grey stripes) is shown in Fig. 8. Two consecutive pulses are separated by a time interval of 1,000 time units.

In the absence of oscillations, the top plate is obviously at rest below the static friction threshold (estimated to be $\mu_{\text{s}} \simeq 0.42$). On the contrary, the vibration pulse can trigger, at the right frequency, long slip events at values of the lateral force well below μ_{s}. But surprisingly there are cases where it has almost no effect on the system (as indicated by the red circle in Fig. 8), corresponding to a value of $\mu \simeq 0.3$.

We have thus performed simulations by adiabatically applying to the top plate, after thermalization, an external force up to a certain value F_{v} (i.e., $\mu_{\text{v}} = F_{\text{v}}/F_{\text{N}}$), below the static threshold μ_{s}, and then keeping it constant. By subsequently applying a vibrating impulse ω_0, we measure the dependence of the plate jump lengths Δ_{slip}, in particular, on the applied stress μ_{v}. Figure 9a displays the details of the X_{top} dynamics of the top plate for an external force $\mu_{\text{v}} = 0.24$ during a short vibration pulse ($T_{\text{v}} = 300$) characterized by the distinct values of ω_0 reported in the inset: inside the frequency range of friction suppression X_{top} usually undertakes long jumps. The lower panel (Fig. 9b) shows the statistical average of the jump, $\langle\Delta_{\text{slip}}\rangle$,

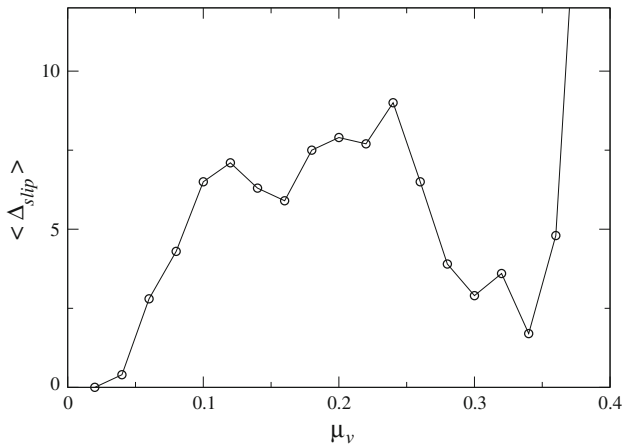

Fig. 10 Average slip length $\langle\Delta_{\text{slip}}\rangle$ as a function of μ_{v} (value of the ratio $F_{\text{v}}/F_{\text{N}}$ when the pulse is applied), for a fixed value of $\omega_0 = 2.4$. Here, $M_{\text{top}} = 60$, $M_{\text{p}} = 177$, $F_{\text{N}} = 60$, $A = 0.2$

as a function of ω_0 for different values of μ_{v}. Contrary to expectations, a larger value of μ_{v} can result in smaller slip jumps Δ_{slip}. An illustrative dependence of the average slip lengths $\langle\Delta_{\text{slip}}\rangle$ on the applied driving μ_{v} is reported in Fig. 10 for an oscillation pulse of duration $T_{\text{v}} = 300$ and frequency $\omega_0 = 2.4$. A peak at $\mu_{\text{v}} \simeq 0.24$ followed by a deep minimum at $\mu_{\text{v}} \simeq 0.34$, highlight an intriguing non-monotonic behavior of $\langle\Delta_{\text{slip}}\rangle$ as a function of μ_{v}.

The corrugated substrate potential generated by the rigid bottom plate can be considered in first approximation sinusoidal. In the window of friction suppression the system (top and confined particles) hops on the bottom plate. Depending on the effective tilting of the corrugated potential (arising from the constant lateral force applied to

the top plate), the oscillating bottom may give a positive (in the direction of the driving) or a negative thrust to the system. Without driving, the top plate simply diffuses, as shown in Sect. 4. Under a small constant force, the top, even if drifting on average in the direction of the applied driving, may get both positive and negative kicks due to the oscillating bottom. But at $\mu_v \approx 0.34$, the positive impulse given by the constant force almost equals the one from the negative thrust. In this situation, the system dwells for a long time in an equilibrium position (moving back and forth) before jumping to a new position. If this dwell time is larger than T_v, the oscillation has almost no effect. For $\mu_v > 0.34$, the system experiences a monotonically decreasing effective potential and it slides smoothly. This aspect surely deserves further investigations.

7 Conclusions

The difficulties of the task in controlling and manipulating friction are related to the complexity of dealing with systems with many degrees of freedom under a strict size confinement, that leaves very limited access to interfere with the sliding interface itself.

In this study, we have analyzed thoroughly and clarified the role of tiny vibrations in the tribological response of a confined system under shear. The general mechanism for friction suppression that we have uncovered is based on the reduction of the effective interface contacts produced by the mechanical actuation. Since the idea is not to change the physical properties of the mating interface, flexibility and accessibility are the main relevant features of this approach: here, frictional properties can be tuned continuously by the frequency and the amplitude of the applied vibrations. The robust results have shown to depend only on the relation between inertial and dissipative forces, and we expect the predicted effects to be valid for a wide class of sliding systems, including granular media and nanoscale interfaces. We have also observed how, in the presence of vibrations, slippage can be favored by small, rather than high, values of the applied shear stress. Further work in this direction could be useful to optimize friction control in technological devices and to design better strategies to forecast the triggering of instabilities in materials and geosystems.

Acknowledgments This study was part of Eurocores Projects FANAS/AFRI, sponsored by the Italian Research Council (CNR), and of FANAS/ACOF, sponsored by the Israel Science Foundation (ISF). It is also sponsored by the Italian PRIN Contracts No. 2008Y2P573. A. Vanossi acknowledges the financial support by SINERGIA Project CRSII2_136287\1 sponsored by the Swiss National Science Foundation. R. Capozza acknowledges the support by the German-Israeli Project Cooperation Program (DIP).

References

1. Persson, B.N.J.: Sliding Friction: Physical Principles and Applications. Springer, Berlin (1998)
2. Persson, B.N.J.: Sliding friction. Surf. Sci. Rep. **33**, 83 (1999)
3. Barel, I., Urbakh, M., Jansen, L., Schirmeisen, A.: Multibond dynamics of nanoscale friction: the role of temperature. Phys. Rev. Lett. **104**, 066104 (2010)
4. Tshiprut, Z., Zelner, S., Urbakh, M.: Temperature-induced enhancement of nanoscale friction. Phys. Rev. Lett. **102**, 136102 (2009)
5. Filippov, A.E., Vanossi, A., Urbakh, M.: Origin of friction anisotropy on a quasicrystal surface. Phys. Rev. Lett. **104**, 074302 (2010)
6. Gao, J., Luedtke, W., Landman, U.: Friction control in thin-film lubrication. J. Phys. Chem. B **102**, 5033 (1998)
7. Rozman, M.G., Urbakh, M., Klafter, J.: Controlling chaotic frictional forces. Phys. Rev. E **57**, 7340 (1998)
8. Zaloj, V., Urbakh, M., Klafter, J.: Modifying friction by manipulating normal response to lateral motion. Phys. Rev. Lett. **82**, 4823 (1999)
9. Tshiprut, Z., Filippov, A.E., Urbakh, M.: Tuning diffusion and friction in microscopic contacts by mechanical excitations. Phys. Rev. Lett. **95**, 016101 (2005)
10. Guerra, R., Vanossi, A., Urbakh, M.: Controlling microscopic friction through mechanical oscillations. Phys. Rev. E **78**, 036110 (2008)
11. Heuberger, M., Drummond, C., Israelachvili, J.N.: Coupling of normal and transverse motions during frictional sliding. J. Phys. Chem. B **102**, 5038 (1998)
12. Socoliuc, A., Gnecco, E., Maier, S., Pfeiffer, O., Baratoff, A., Bennewitz, R., Meyer, E.: Atomic-scale control of friction by actuation of nanometer-sized contacts. Science **313**, 207 (2006)
13. Jeon, S., Thundat, T., Braiman, Y.: Effect of normal vibration on friction in the atomic force microscopy experiment. Appl. Phys. Lett. **88**, 214102 (2006)
14. Su, L., Xu, J., Kurita, M., Kato, K., Adachi, K.: Tapping effect on friction between slider and disk. Tribol. Lett. **15**, 91 (2003)
15. Johnson, P.A., Savage, H., Knuth, M., Gomberg, J., Marone, C.: Effects of acoustic waves on stick–slip in granular media and implications for earthquakes. Nature **451**, 57 (2008)
16. Capozza, R., Vanossi, A., Vezzani, A., Zapperi, S.: Suppression of friction by mechanical vibrations. Phys. Rev. Lett. **103**, 085502 (2009)
17. Urbakh, M., Klafter, J., Gourdon, D., Israelachvili, J.: The nonlinear nature of friction. Nature **430**, 525 (2004)
18. Braun, O.M., Naumovets, A.G.: Nanotribology: microscopic mechanisms of friction. Surf. Sci. Rep. **60**, 79 (2006)
19. Vanossi, A., Braun, O.M.: Driven dynamics of simplified tribological models. J. Phys. Condens. Matter **19**, 305017 (2007)
20. Benassi, A., Vanossi, A., Santoro, G.E., Tosatti, E.: Parameter-free dissipation in simulated sliding friction. Phys. Rev. B **82**, 081401(R) (2010)
21. Kowalik, Z.J., Franaszek, M., Pierański, P.: Self-reanimating chaos in the bouncing-ball system. Phys. Rev. A **37**, 4016 (1988)
22. Mehta, A., Luck, J.M.: Novel temporal behavior of a nonlinear dynamical system: the completely inelastic bouncing ball. Phys. Rev. Lett. **65**, 393 (1990)
23. Luck, J.M., Mehta, A.: Bouncing ball with a finite restitution: chattering, locking, and chaos. Phys. Rev. E **48**, 3988 (1993)
24. Mátyás, L., Klages, R.: Irregular diffusion in the bouncing ball billiard. Phys. D **187**, 165 (2004)
25. de Wijn, A.S., Kantz, H.: Vertical chaos and horizontal diffusion in the bouncing-ball billiard. Phys. Rev. E **75**, 046214 (2007)
26. Dalton, F., Farrelly, F., Petri, A., Pietronero, L., Pitolli, L., Pontuale, G.: Shear stress fluctuations in the granular liquid and solid phases. Phys. Rev. Lett. **95**, 138001 (2005)